INVESTIGATION OF NUCLEATION MECHANISMS OF NANOCRYSTALLINE PYROCHLORE PHOSPHORS EMITTING IN INFRARED

[1]Ivo BARTOŇ, [1]Soňa KAMRÁDKOVÁ, [1]Jana PROBOŠTOVÁ, [2]Luminita PREDOANA, [2]Jeanina PANDELE-CUSU, [1]Jan MRÁZEK

[1]*Institute of Photonics and Electronics of the Czech Academy of Sciences, Prague, Czech Republic, EU,* barton@ufe.cz

[2]*"Ilie Murgulescu" Institute of Physical Chemistry, Bucharest, Romania, EU,* lpredoana@icf.ro

https://doi.org/10.37904/nanocon.2022.4573

Abstract

High-power infrared lasers are the heart of modern equipment in telecommunications, tracking and navigation systems, etc. The increasing power of lasers places high demands on the materials used as active laser media, which must exhibit high thermal stability and luminescence efficiency. Rare earth-doped yttrium titanium oxides, with the general formula $(RE_xY_{1-x})_2Ti_2O_7$, represent a perspective class of materials for their phenomenal optical properties. Because the optical properties are highly sensitive to the structure and uniformity of the nanocrystals constituting the material, the knowledge of crystallization kinetics is necessary to prepare the nanocrystalline materials with tailored properties. We present a versatile sol-gel approach to nanocrystalline $Y_2Ti_2O_7$ and $(Er_{0,05}Y_{0,95})_2Ti_2O_7$. We studied the nucleation process and crystallization mechanism of $Y_2Ti_2O_7$ and $(Er_{0.05}Y_{0.95})_2Ti_2O_7$ from the amorphous xerogels. The crystallization temperatures of $Y_2Ti_2O_7$ and $(Er_{0,05}Y_{0,95})_2Ti_2O_7$ were 792.5 ± 0.9 and 789.9 ± 0.5 °C, respectively. Based on calculated Avrami parameters the formation of $Y_2Ti_2O_7$ from amorphous xerogel was driven by homogenous site-saturated nucleation. The introduction of Er^{3+} ions into host lattice of $Y_2Ti_2O_7$ changed the crystallization kinetics causing the formation of $(Er_{0.05}Y_{0.95})_2Ti_2O_7$ occurred in a manner of homogenous nucleation with a constant nucleation rate. The different crystallization kinetics caused the nanocrystals of $(Er_{0.05}Y_{0.95})_2Ti_2O_7$ to be larger and exhibited broader nanocrystals size distribution than the nanocrystals of undoped $Y_2Ti_2O_7$. The results provide fundamental information about nucleation and growth properties and crystal structure of investigated luminophores and give necessary information for preparing nanocrystalline powders with tailored properties for high-power photonic devices.

Keywords: Nucleation, crystallization, pyrochlore, phosphors, $(Er_{0.05}Y_{0.95})_2Ti_2O_7$

1. INTRODUCTION

Lanthanide titanium oxides, crystallizing in a pyrochlore structure with a general formula $A_2B_2O_7$ [1], have attracted attention in recent material research for their magnetic and optical properties. The spin arrangement of rare earths (RE) in the pyrochlore lattice provides distinctive magnetic properties allowing the preparation of spin-glass and spin-ice compounds [2,3]. Although the $RE_2B_2O_7$ pyrochlores are optically inactive, the yttrium ions in the pyrochlore structure break the spin interactions and prevent the non-radiative transitions between RE ions [4,5]. Consequently, the RE-doped $Y_2Ti_2O_7$ exhibit effective luminescence properties and they have been intensively studied as luminophores for high-power photonic applications [6,7]. The final optical properties of RE-doped $Y_2Ti_2O_7$ strongly depend on the local arrangement and regular distribution of RE ions inside the crystal lattice. The local clustering of RE ions supports the non-radiative transitions and reduces the luminescence efficiency. The structural defects and broad nanocrystal size distribution can contribute to the scattering of the light and increase the optical losses [8,9]. Therefore, the processing of RE-doped $Y_2Ti_2O_7$

must be carefully tailored to keep the regular statistical distribution of RE inside the pyrochlore lattice and to prepare highly homogenous luminophores or coatings [6,7].

Several approaches have been used for the synthesis of pyrochlores. In addition to standard high-temperature sintering ceramic methods [1,2], the “bottom-up” sol-gel methods have been intensively studied to prepare broad set of luminescent powders [6,10] and active optical waveguides [7,11]. The “bottom-up” methods benefit from targeted thermally induced crystallization of amorphous materials. However, the processing temperature must be carefully controlled to prevent the side-formation of parasitic phases or unwanted nanocrystal overgrowth. Knowledge of the crystallization kinetics of pyrochlores from amorphous precursors opens up possibilities for extending the synthesis of RE-doped $Y_2Ti_2O_7$ and preparing the luminophores with tailored structural properties.

This study presents a versatile sol-gel approach to nanocrystalline $Y_2Ti_2O_7$ and $(Er_{0.05}Y_{0.95})_2Ti_2O_7$. We evaluated the structural properties of prepared nanocrystals. We study the nucleation process and crystallization mechanism of $Y_2Ti_2O_7$ and $(Er_{0.05}Y_{0.95})_2Ti_2O_7$ from the amorphous xerogels. The acquired knowledge is necessary for the preparation of nanocrystalline powders with tailored properties for high-power photonic devices.

2. EXPERIMENTAL

The samples were prepared by a sol-gel method followed by thermal treatment of the xerogels. To prepare the sols, a total of 5 g titanium(IV)butoxide (Fluka, Purum) was dissolved in 250 ml of anhydrous ethanol (Sigma–Aldrich, Spectranal grade), after which a total of 5.63 g of yttrium(III) nitrate hexahydrate (Aldrich, 99.8%), or a total of 5.35 g yttrium(III) nitrate hexahydrate (Aldrich, 99.8%) and 0.325 g of erbium(III) nitrate pentahydrate (Aldrich, 99.9%) were dispersed in the solution. The mixtures were stirred at ambient temperature to form the transparent solutions, which were refluxed at 80 °C for 24 h and then allowed to cool. The sols were dried on a rotary evaporator (R100, Buchi) to form the xerogels.

Differential thermal analysis (DTA) and thermal gravimetry (TG) measurements were performed using a Mettler Toledo TGA/SDTA 851^e apparatus. The samples were analyzed in alumina crucibles at heating rates ranging from 10 to 40 °C·min^{-1} under an oxygen flow of 50 ml·min^{-1}.

X-ray powder diffraction (XRD) patterns were collected using a Bruker D8 Discover diffractometer in the Bragg-Brentano reflecting geometry. The copper tube was operated at voltage of 40 kV and current of 40 mA providing Cu-Kα1 radiation (λ=1.540596 Å).

Scanning electron microscopy (SEM) images were obtained with a TESCAN Lyra 3 XMU device. A thin carbon layer was sputtered onto the samples to prevent sample charging. To evaluate the nanocrystal size distribution, we marked the nanocrystal boundaries in the SEM images and we used Gwyddion 2.55 data visualization and analysis software.

3. RESULTS AND DISCUSSION

The thermal processing of xerogels represents a complex process consisting of a broad set of physical and chemical processes. It usually includes several steps involving the evaporation of volatile substances, burning and decomposition of organic compounds and inorganic ligands, and the crystallization process itself. A key factor for the successful synthesis of pyrochlores with tailored structural properties is a perfect knowledge of the physicochemical processes occurring during thermal treatment. **Figure 1a** shows the general thermal analysis curves recorded for the heat rate of 40 °C·min^{-1}. DTA curve shows broad endothermic peak below 300 °C and two exothermic peaks around 350 °C and 843 °C. The broad endothermic peaks below 600 °C and the first exothermic peak around 350 °C were accompanied by regular weight loss. The minor weight loss accompanied the second exothermic peak at 820 °C. According to the chemical analysis of the compounds liberated during the thermal treatment of pyrochlores, the broad endothermic peak below 300 °C can be attributed to the liberation of water, vaporization, and carbonization of the adsorbed alcohols and esters [12].

The exothermic peak around 350 °C was attributed to the decomposition of nitrates and the condensation of -OH groups presented in the xerogels [13,14]. The remaining nitrates act as complexing agents that stabilized Y^{3+} and RE^{3+} ions inside the amorphous titanium dioxide matrix preventing the crystallization of titanium dioxide [14]. Once the nitrates are burn-out the crystallization of pyrochlores takes place. The burning-out of the nitrates was attributed to mass loss at 820 °C and the minor exothermic peak at 843 °C corresponded to the crystallization of $Y_2Ti_2O_7$.

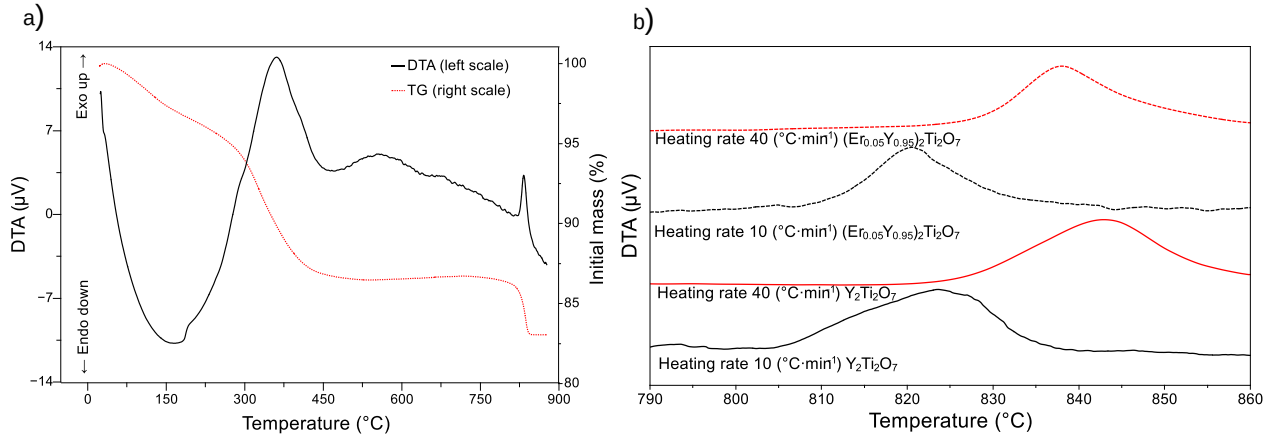

Figure 1 Representative results of thermal analysis. a) Differential thermal analysis and thermal gravimetry records for $Y_2Ti_2O_7$ powder recorded for heating rate of 40 °C·min^{-1}. b) Zoom on the DTA curves demonstrating the shift of the crystallization peaks with different heating rates

The crystallization is a dynamic process depending on the overheating or overcooling of the thermally treated materials. The shape and position of the crystallization peak depend on the heating rate of the analyzed samples. **Figure 1b** shows the shifts in the positions of representative crystallization peaks in detail. The crystallization of $Y_2Ti_2O_7$ occurs at 824.6 °C for the heating rate of 10 °C·min^{-1}. With increasing heating rates, the positions of the crystallization peaks shift to higher temperatures and the peaks became better pronounced. Compared with $Y_2Ti_2O_7$, the crystallization peaks of $(Er_{0,05}Y_{0,95})_2Ti_2O_7$ shifted to lower temperatures.

The shifts in the positions of crystallization peaks have been used in many theoretical and experimental models to evaluate fundamental crystallization parameters. The crystallization temperature of nanocrystalline materials, t_c, can be calculated using the empirical Lasocka's equation [15]:

$$t_p = t_c + A_c \cdot \ln(\alpha) \quad (1)$$

where t_p represents the position of the crystallization peak (°C), α is the heating rate (°C·min^{-1}), and A_c is the experimental constant. **Figure 2a** shows the experimental positions of the crystallization peaks for various heating rates and corresponding linear fits. The y-intercept representing t_c was calculated from a linear fit of α equal to 1 °C·min^{-1}. The crystallization temperatures of $Y_2Ti_2O_7$ and $(Er_{0,05}Y_{0,95})_2Ti_2O_7$ were 792.5 ± 0.9 and 789.9 ± 0.5 °C, respectively. These values were in line with the crystallization temperatures of pyrochlores prepared by Pechini's methods, e.g. 817.7 °C for $Er_2Ti_2O_7$ [16], 821 °C for $Y_2Ti_2O_7$ [17], and ~800 °C for Er-doped $Y_2Ti_2O_7$ [18].

XRD records of the samples heat-treated at 1000 °C are shown in **Figure 2b**. The pure pyrochlore cubic phase of $Y_2Ti_2O_7$ was formed and the crystal lattice parameter a of $Y_2Ti_2O_7$ was 10.0963 Å. This value matches the value of 10.0976 Å reported for single-crystal sample [17]. The XRD pattern of $(Er_{0,05}Y_{0,95})_2Ti_2O_7$ exhibited isostructural diffraction lines confirming the formation of the pyrochlore structural type. The samples were free of side-formed oxides, such as TiO_2, Y_2O_3, or $Er_2Ti_2O_7$, and the diffraction lines did not show the twining, proving the regular statistical distribution of Er^{3+} ions inside the pyrochlore crystal lattice. The positions of the diffraction lines were shifted to longer angles providing the crystal lattice parameter a = 10.1071 Å.

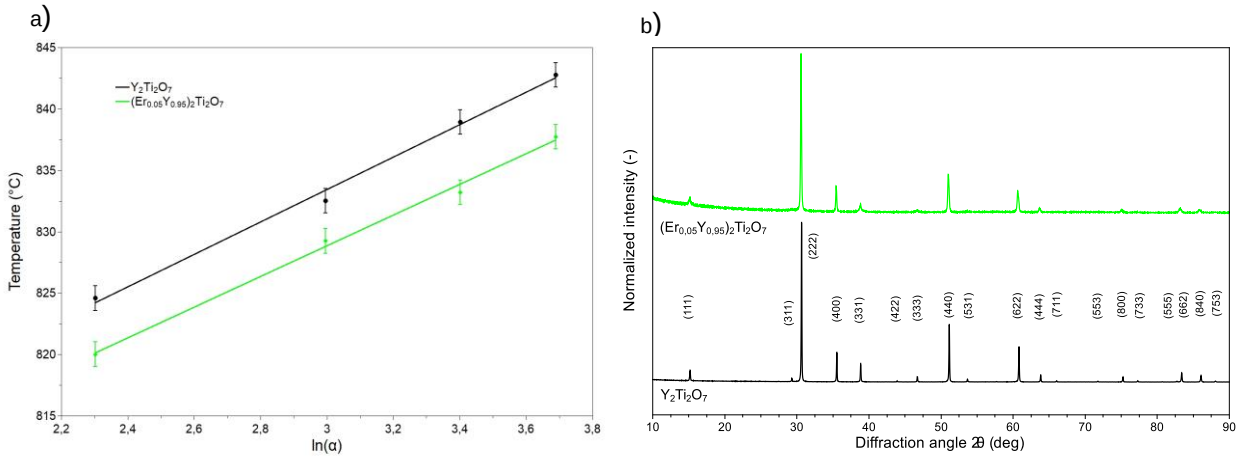

Figure 2 a) Linear fits of Lasocka's equation approximating the crystallization temperature of the compounds. b) Diffractograms of the prepared compounds heat-treated at 1000 °C

To determine the crystallization kinetics, we used Johnson, Mehl, and Avrami model (JMA). In the JMA approximation, the relationship between the crystallization rate, $d\psi/d\tau$, and volume fraction of crystallized material, ψ, at time, τ, can be expressed in the general form of the JMA kinetic equation:

$$\frac{d\psi}{d\tau} = k \cdot \eta \cdot (1-\psi) \cdot [-ln(1-\psi)]^{1-\frac{1}{\eta}} \quad (2)$$

where η is the Avrami parameter that depends on the nucleation and growth mechanism, k is the rate constant, and volume fraction of crystallized material, ψ, is also known as the relative crystallinity of the sample crystallized at time τ (min). A representative course of relative crystallinity is shown in **Figure 3a**.

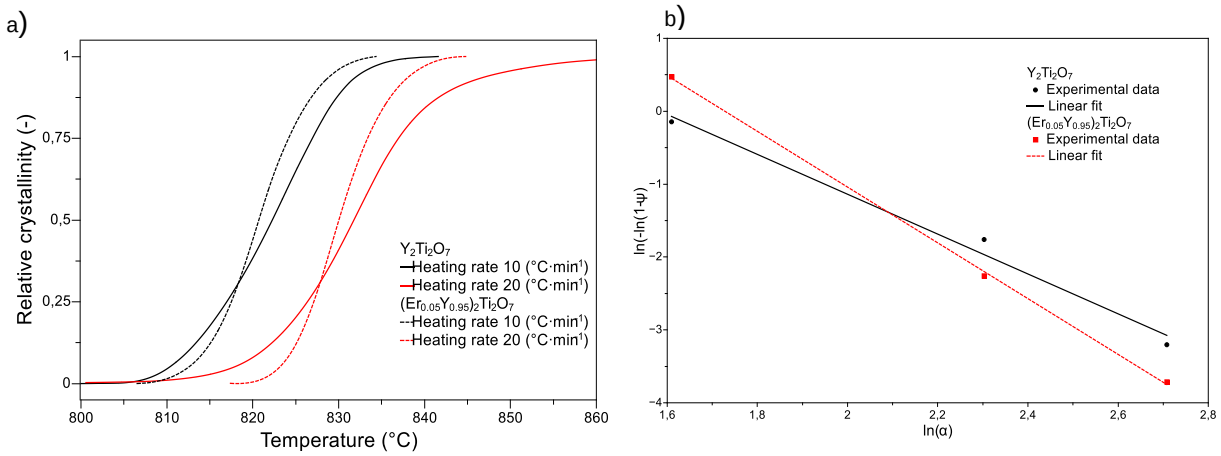

Figure 3 a) Variation of the relative crystallinity with heating rate for particular compounds. b) Logarithmic plot of the dependence of the term *-ln(1-Ψ)* on the heating rate for the evaluation of Avrami parameters for the non-isothermal crystallization kinetics approach.

The positions of the curves shifted to higher temperatures with increasing heating rates. The curves' slopes increased with increasing dimensionality of the nucleation process and the crystal growth [19]. For linear heating rates the JMA kinetic equation can be expressed by the Ozawa's non-isothermal modification [20]:

$$-\eta = \frac{d\{ln[-ln(1-\psi)]\}}{d\ ln\ a}\Big|_{t_a} \quad (3)$$

where the Avrami parameter η, is determined from the slope of the plot of ln[–ln(1–ψ)] vs. ln α. The relative crystallinity, ψ, is calculated as the ratio of the partial integration area of the crystallization peak at temperature

t_a to the total area of the crystallization peak. **Figure 3b** shows the corresponding data and fits allowing evaluation of the Avrami parameters, which were 2.9 ± 0.3 and 4.1 ± 0.2 for $Y_2Ti_2O_7$ and $(Er_{0.05}Y_{0.95})_2Ti_2O_7$, respectively. The values of the Avrami parameter are characteristic of particular nucleation mechanism and mass transfer causing the nanocrystal growth [16,21]. Each dimension of the crystal growth or formation of nuclei contributes a unit to the total Avrami parameter. Therefore, the values corresponding to homogenous nucleation with a constant nucleation rate are greater by a unit than those corresponding to site-saturated nucleation. Because the real crystallization process usually combines several mechanisms, the Avrami parameters slightly differ from the predicted theoretical integers. The value of η calculated for $Y_2Ti_2O_7$ matched the value of 2.8 reported for $Y_2Ti_2O_7$ prepared by Pechini's method [17]. The excellent agreement of these results suggested that the crystallization mechanism of $Y_2Ti_2O_7$ from the amorphous "soft chemistry" precursors is identical and the pyrochlores crystallize in a manner of homogenous 3-D site-saturated nucleation. However, the introduction of Er^{3+} ions significantly increased the value of the Avrami parameter up to 4. Such a high value suggested that the crystallization of $(Er_{0.05}Y_{0.95})_2Ti_2O_7$ runs in a manner of homogenous nucleation with a constant nucleation rate.

The different crystallization kinetics have a significant effect on the nanocrystalline structure of the prepared materials. To verify the proposed crystallization mechanism, the powders heat-treated at 1000 °C for 30 minutes were visualized by SEM and the images are shown in **Figure 4**. The powder of $Y_2Ti_2O_7$ was composed of well-grown nanocrystals with a regular shape without any preferential size orientation. **Figure 4c** shows that the nanocrystal diameter ranged from 50 to 200 nm with a mean diameter of 100 nm. Uniform and narrow nanocrystal size distribution is typical for sited-saturated nucleation. Nuclei are formed in the entire volume of the amorphous material at once in a very narrow temperature interval. The prolongated thermal treatment promotes the recrystallization of the material, causing the nanocrystal size distribution to broaden and grow. In the case of $(Er_{0.05}Y_{0.95})_2Ti_2O_7$, the observed variability of the nanocrystal size and shape was higher than for $Y_2Ti_2O_7$. The nanocrystals were larger, the smaller nanocrystals filled the spaces between larger one and the nanocrystal diameter ranged from 25 to 325 nm with a mean frequency of 175 nm. A broad nanocrystal size distribution is typical for homogenous nucleation with a constant nucleation rate. The nuclei formed at the beginning of the crystallization process regularly grew into larger nanocrystals. Simultaneously, the nucleation of new, smaller nanocrystals occurs. The final materials consist of nanocrystals with broad size distribution.

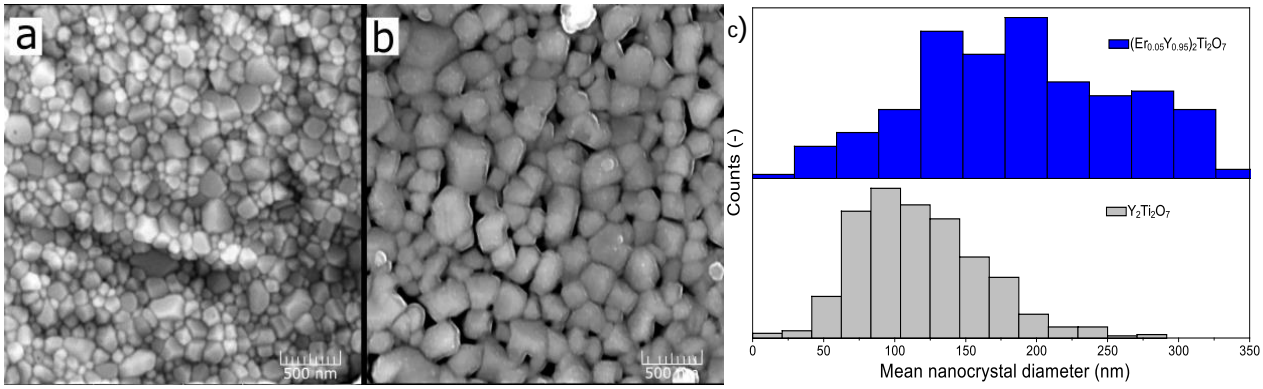

Figure 4 SEM image of the compounds heat-treated at 1000 °C. a) Sample of $Y_2Ti_2O_7$. b) Sample of $(Er_{0.05}Y_{0.95})_2Ti_2O_7$. c) Histogram summarizing the nanocrystal size distribution

The presented Avrami parameters and nanocrystal size analyses supported the conclusion that the introduction of RE into the host matrix of $Y_2Ti_2O_7$ changed the crystallization mechanism and the crystallization process of $(Er_{0.05}Y_{0.95})_2Ti_2O_7$ occurred in the manner of homogenous nucleation with a constant nucleation rate. The homogenous nucleation with constant nucleation rate can reduce the associated energy consumption due to the lower nucleation energy barrier [22]. However, the broad nanocrystal size distribution can increase the Rayleigh scattering. This phenomenon can reduce the optical quality of prepared materials and limit their application in photonics [23,24].

4. CONCLUSION

We demonstrated a sol-gel approach to nanocrystalline $Y_2Ti_2O_7$ and $(Er_{0.05}Y_{0.95})_2Ti_2O_7$. The crystallization temperatures of $Y_2Ti_2O_7$ and $(Er_{0.05}Y_{0.95})_2Ti_2O_7$ were 792.5 ± 0.9 and 759.9 ± 0.5 °C, respectively. The Er^{3+} ions statistically substituted the Y^{3+} ions inside the pyrochlore structural lattice causing the increase of the crystal lattice parameter *a* up to 10.1071 Å. We used the non-isothermal crystallization kinetics approach and image analysis of SEM to evaluate the crystallization mechanisms. The crystallization of $Y_2Ti_2O_7$ occurred in the manner of site-saturated nucleation. The introduction of Er^{3+} ions into the host lattice of $Y_2Ti_2O_7$ changed the nucleation mechanism and $(Er_{0.05}Y_{0.95})_2Ti_2O_7$ crystallized in the manner of homogenous nucleation with a constant nucleation rate. The acquired knowledge is necessary to prepare nanocrystalline powders with tailored properties for high-power photonic devices.

ACKNOWLEDGEMENTS

This research was financially supported by the Czech Science Foundation number 22-14200S and the mobility project of the Czech Academy of Sciences number AR-20-01.

REFERENCES

[1] GLERUP, M., NIELSEN, O. F., POULSEN, F. W. The structural transformation from the pyrochlore structure, A(2)B(2)O(7), to the fluorite structure, AO(2), studied by Raman spectroscopy and defect chemistry modeling. *Journal of Solid State Chemistry*. 2001, vol. 160, no. 1, pp.25-32

[2] GARDNER, J. S., GINGRAS, M.J., GREEDAN, J.E. Magnetic pyrochlore oxides. *Reviews of Modern Physics*. 2010, vol. 82, no. 1, pp. 53–107.

[3] VLASKOVA, K., PROSCHEK, P., DIVIS, M., Duc, L.E., COLMAN, R.H., KLICPERA, M. Magnetic properties and crystal field splitting of the rare-earth pyrochlore $Er_2Ir_2O_7$. *Physical Review B*. 2020, vol. 102, vol. 5.

[4] JENOUVRIER, P., BOCCARDI, G., FICK, J., JURDYC, A. M., LANGLET, M. Up-conversion emission in rare earth-doped $Y_2Ti_2O_7$ sol–gel thin films. *Journal of Luminescence*. 2005, vol. 113, no. 3–4, pp. 291–300.

[5] SINGH, B. P., PARCHUR, A. K., SINGH, R. K., ANSARI, A. A., SINGH, P., RAI, S. B. Structural and up-conversion properties of Er^{3+} and Yb^{3+} co-doped $Y_2Ti_2O_7$ phosphors. *Physical Chemistry Chemical Physics* [online]. 2013, vol. 15, no. 10, pp. 3480–3489.

[6] GUO, Y., WANG, D., ZHAO, X., WANG, F. Fabrication, microstructure and upconversion luminescence of Yb^{3+}/Ln(3+) (Ln=Ho, Er, Tm) co-doped $Y_2Ti_2O_7$ ceramics. *Materials Research Bulletin*. 2016, vol. 73, pp. 84–89.

[7] VYTYKACOVA, S., MRAZEK, J., PUCHY, V., DZUNDA, R., SKALA, R., PETERKA, P., KASIK, I. Sol-gel route to highly transparent $(Ho_{0.05}Y_{0.95})(2)Ti_2O_7$ thin films for active optical components operating at 2 mu m. *Optical Materials Express*. 2018, vol. 78, pp. 415–420.

[8] ALMEIDA, R. M., MARQUES, A. C., PORTAL, S. Glassy and nanocrystalline photonic materials and structures by sol–gel. *Optical Materials*. 2005, vol. 27, no. 11, pp. 1718–1725.

[9] MATEJEC, V., MRAZEK, J., HAYER, M., KASIK, I., PETERKA, P., KANKA, J., HONZATKO, P., BERKOVA, D. Microstructure fibers for gas detection. *Materials Science & Engineering C-Biomimetic and Supramolecular Systems*. 2006, vol. 26, no. 2–3, SI, pp. 317–321.

[10] JENOUVRIER, P., FICK, J., AUDIER, M., LANGLET, M. Microstructure and photoluminescence properties of sol–gel $Y_{2-x}Er_xTi2O_7$ thin films. *Optical Materials*. 2004, vol. 27, no. 2, pp. 131–137.

[11] JENOUVRIER, P., LANGLET, M., RIMET, R., FICK, J. Influence of crystallisation on the photoluminescence properties of $Y_{2-x}Er_xTi_2O_7$ sol-gel thin films. *Applied Physics a-Materials Science & Processing*. 2003, vol. 77, no. 5, pp. 687–692.

[12] STARUKH, G., TOSCANI, S., BOURSICOT, S., SPANHEL, L. Photoactivity of sol-gel derived nitridated ZnxTiyOz-films. *Zeitschrift Fur Physikalische Chemie-International Journal Of Research In Physical Chemistry & Chemical Physics*. 2007, vol. 221, no. 3, pp. 349–360.

[13] BALTRUSAITIS, J., SCHUTTLEFIELD, J., JENSEN, J.H., GRASSIAN, V.H. FTIR spectroscopy combined with quantum chemical calculations to investigate adsorbed nitrate on aluminium oxide surfaces in the presence and absence of co-adsorbed water. *Physical Chemistry Chemical Physics*. 2007, vol. 9, no. 36, pp. 4970–4980.

[14] MRAZEK, J., POTEL, M., BURSIK, J., MRACEK, A., KALLISTOVA, A., JONASOVA, S., BOHACEK, J., KASIK, I. Sol-gel synthesis and crystallization kinetics of dysprosium-titanate Dy2Ti2O7 for photonic applications. *Materials Chemistry and Physics*. 2015, vol. 168, pp. 159–167.

[15] LASOCKA, M. Effect of scanning rate on glass-transition temperature of splat-cooled Te-85-Ge-15. *Materials Science and Engineering*. 1976, vol. 23, no. 2–3, pp. 173–177.

[16] MILICEVIC, B., KUZMAN, S., POROBIC, S. J., MARINOVIC-CINCOVIC, M., DRAMICANIN, M. D. Non-isothermal crystallization kinetics of the heavy-group lanthanide dititanates. *Optical Materials*. 2017, vol. 74, pp. 86–92.

[17] MILICEVIC, B., MARINOVIC-CINCOVIC, M., DRAMICANIN, M. D. Non-isothermal crystallization kinetics of Y(2)Ti(2)O7. *Powder Technology*. 2017, vol. 310, pp. 67–73.

[18] TING, C.C., CHIU, Y.S., CHANG, C.W., CHUANG, L.C. Visible and infrared luminescence properties of Er^{3+}-doped $Y_2Ti_2O_7$ nanocrystals. *Journal of Solid State Chemistry*. 2011, vol. 184, no. 3, pp. 563–571.

[19] VAZQUEZ, J., GONZALEZ-PALMA, R., VILLARES, P., JIMENEZ-GARAY, R. Theoretical study on the glass-crystal transformation and deduction of its kinetic parameters by DSC, using non-isothermal regime. *Physica B-Condensed Matter*. 2003, vol. 336, no. 3–4, pp. 297–307.

[20] MALEK, J., MITSUHASHI, T. Testing method for the Johnson-Mehl-Avrami equation in kinetic analysis of crystallization processes. *Journal of the American Ceramic Society*. 2000, vol. 83, no. 8, pp. 2103–2105.

[21] PEREZ-MAQUEDA, L. A., CRIADO, J.M., J. MALEK, J. Combined kinetic analysis for crystallization kinetics of non-crystalline solids. *Journal of Non-Crystalline Solids*. 2003, vol. 320, no. 1–3, pp. 84–91.

[22] YASNO, J. P., CONCONI, S., VISINTIN, A., SUAREZ, G. Non-isothermal reaction mechanism and kinetic analysis for the synthesis of monoclinic lithium zirconate (m-Li2ZrO3) during solid-state reaction. *Journal of Analytical Science and Technology*. 2021, vol. 12, no. 1.

[23] ALMEIDA, R. M., MARQUES, A.C., CHIASERA, A., CHIAPPINI, A., FERRARI, M. Rare-earth doped photonic crystal microcavities prepared by sol–gel. *Journal of Non-Crystalline Solids*. 2007, vol. 353, no. 5, pp. 490–493.

[24] KASIK, I., MRAZEK, J., PODRAZKY, O., SEIDL, M., AUBRECHT, J., TOBISKA, P., POSPISILOVA, M., MATEJEC, V., KOVACS, B., MARKOVICS, A., SZILI, M. Fiber-optic detection of chlorine in water. *Sensors and Actuators B-Chemical*. 2009, vol. 139, no. 1, pp. 139–142.